

## **Investigations of heat-transfer rate and surface pressure distribution over a sharp cone model at hypersonic Mach number**

M.Saiprakash<sup>a,\*</sup>, C.Senthilkumar<sup>b</sup>, Kadam sunil.G<sup>c</sup>, Singh Prakash Rampratap<sup>c</sup>,  
Shanmugam.V<sup>c</sup>, Balu .G<sup>c</sup>

<sup>a</sup>*Department of Aerospace Engineering, MLR institute of technology, Telengana-500043, Hyderabad, India*

<sup>b</sup>*Department of Aerospace Engineering, MIT Campus, Anna University, Chennai,600044,India*

<sup>c</sup>*Directorate of Aerodynamics, Defence Research & Development Laboratory, Hyderabad ,500058, India*

\*Corresponding author Email: iamsaiaero@gmail.com

Experiments were carried in a hypersonic shock tunnel to obtain the convective heating rate and surface pressure distribution on a sharp cone model placed at hypersonic speed. Test was carried out at flow Mach number of 6.56 at a stagnation enthalpy of 1.2 MJ/kg. Helium used as driver gas and air as the test gas. The effective test time during tunnel testing is 3.5 ms. The flow establishment, steady state, and termination process of the hypersonic flow have been visualized from schlieren image for a flow Mach number of 6.5 at two different angles of attack 0° & 5°. The vacuum sputtered thin film platinum sensors are used to measure the heat flux on a model surface. The measured heat transfer rate compares well with computational fluid dynamics simulation. The measured surface pressure compares well with computational fluid dynamics .

**Keywords:** shock tunnel, heat transfer, cone model

### **1. Introduction**

In hypersonic flows, the knowledge of stagnation and surface heat transfer rate for a vehicle configuration is essential to quantify the heat shielding requirement for the thermal protection system of a vehicle. The heat transfer to the body surface is function of body shape and flight conditions. Surface pressure distribution is an important parameter which influences the aerodynamic drag therefore it needs to be measured. In hypersonic flight regime, intrinsic complexity arises in flow aerothermodynamics around the vehicle at the Mach number exceeding 5 due to effects such as thin shock layer, entropy layer, viscous interaction, chemically reacting boundary layers, dissociated high-temperature flows and regime of low density flow.

The advantage of the sharp cone model is that the shock wave in the leading edge is attached at the nose, thus the flow behind the sharp cone model does not leak around the leading from bottom to top surface. But in the blunt cone model, the shock wave is detached around the leading edge, hence there is the possibility of flow behind the shock being leaked around the leading edge. Hence higher integrated pressure over the bottom surface is preserved and high lift is generated on the sharp cone model compared with the blunt cone model where relatively lower integrated bottom surface pressure and reduced lift prevail. Therefore, the vehicle having blunt cone shape must fly at higher angle of attack to produce the same lift as the sharp cone shape.

In a blow down facility, the hypersonic Mach number in the test section is achieved by decreasing the free stream temperature which results in decreasing the speed of sound and leading to corresponding increase in the flow Mach number. In a Blow down type wind Tunnel capable to produce high flow Mach number but upper limit on the Mach number is imposed for a given reservoir temperature by condensation of the test gas in the test section.

Hornung (1988) experimentally investigated that conventional blow down facility incorrectly simulate the real gas effect for a flow Mach number above 6. Real gas effects can be successfully

simulate in shock tunnel by producing air flow in the test section with energy matching that in flight of the hypersonic vehicle. This can be achieved by expanding the test gas from the end of shock tube at very high temperature and pressure through a convergent divergent nozzle. Aero braking [2] is the best manoeuvre of planet's atmosphere to decelerate upon the entry. The prime advantage of aero assisted manoeuvres is substantial amount of saving of propellant required for a mission and it allows greater payload to be installed. In most of the inter-planetary space missions, large angle blunt bodies ( $\sim$  semi-apex angle  $60^\circ$  or  $70^\circ$ ) having low lift to drag bodies are employed to provide effective heat shield in aero assisted orbital transfer vehicles.

Over the years, several heat transfer measurements over a blunt cone model have been reported in the open literature by Micol (1995) , Tauber (1993) , Raju, I.S and Craft, W.J (1993). Thermographic phosphorus (De Luca,1995), infrared thermographs(Mico11995) and temperature sensitive paint(Hubner 2001) techniques are used to measure the heat transfer measurement. In the present study, platinum thin film sensors are used to measure heat flux on model.

The shock tunnel in DRDL(Defence Research &Development Laboratory) can produce hypersonic Mach number from 6 to 10 by using different throat sections, Maximum working pressure and maximum temperature of the tunnel are 100bar and 4000K respectively(chandra 2007). The prime objective of the present study 1) to measure and investigate the surface heat transfer and surface pressure distribution for sharp cone model at  $0^\circ$  &  $5^\circ$  angle of attacks. 2) to validate the experimental results with theoretically estimated values using Reference enthalpy method and CFD simulation.

## 2.EXPERIMENTAL FACILITY

Shock tunnel consists of shock tube, convergent divergent nozzle, test section/dump tank. The total length of the shock tunnel was 31.7 m. The lengths of the driver section and the driven section were 5 m and 18.7 m respectively and both were made of stainless steel. The internal diameter of shock tube is 180 mm. The shorter section and the longer section were separated by an aluminium diaphragm and it had the thickness of 6.4 mm, groove depth of 2.8 mm, and groove length of 200 mm. Similarly shock tube and the C-D nozzle were separated by Mylar diaphragm. The driven section and the test section/dump tank were evacuated from 1 bar to 0.5 bar and  $1 \times 10^{-6}$  mbar respectively. Sharp cone model size of 150 mm diameter can be tested in the inviscid core of 5 m test section. Nozzle exit diameter of 590 mm is used for generating the hypersonic flow over the test model by operating the tunnel in the reflected mode. Based on the Pitot rake calibration runs, the test flow Mach number is estimated as 6.5 during the steady flow of 3.5 ms. Figure 1 shows layout of hypersonic shock tunnel.

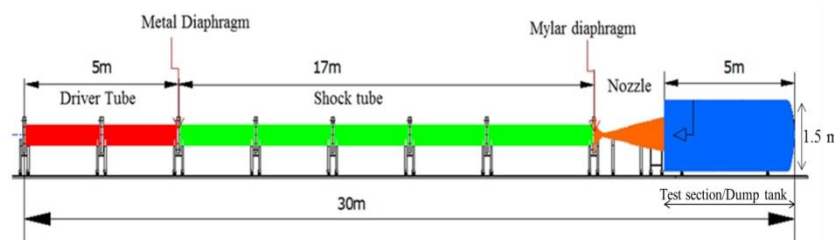


Fig. 1 Layout of hypersonic shock tunnel

### 2.1. Transient flow in shock tube

The tunnel has provision for mounting five Pressure transducer in the shock tube, out of five, four PCB Pressure transducers are used for measurement. The first PCB pressure transducer(SSP2) is at the 15.378 m downstream of aluminium diaphragm, and another two pressure transducers

(SSP3 & SSP4) are mounted at 892 mm and 532 mm from mylar diaphragm. The last pressure measurement ( $P_{05}$ ) is used as a Nozzle reservoir condition of the system which is mounted very close to mylar diaphragm. In the present experiment, pressure transducers used are 113A24 (model number 18823), sensitivity 71.79 mV/bar and 113A24 (18825), sensitivity 72.95 mV/bar for SSP4 and SSP5 pressure sensors respectively. The above sensors have high bandwidth of 250 KHz and rise time of 1-2  $\mu$ s. Fig 2 shows sensor location in the shock tube.

The pressure histories in Fig 3 follow the flow physics inside the shock tube. The incident shock wave increases the pressure to 5 bar. As the shock progresses to the end of mylar diaphragm and reflects towards driver section, it further increases the pressure to 24 bar. Theoretical estimated incident shock pressure and reflected shock pressure are 5.5 and 24.6 bar respectively. The constant steady state flow duration is about 3.4 ms which is between 0.031 and 0.035s as measured by  $P_{05}$  pressure transducer as shown in Fig 3. The sudden decrease in the pressure after 0.035s could be due to interaction of shock wave with contact surface or due to interaction of reflected expansion wave that travels to the left into the reservoir, catching up with the end section.

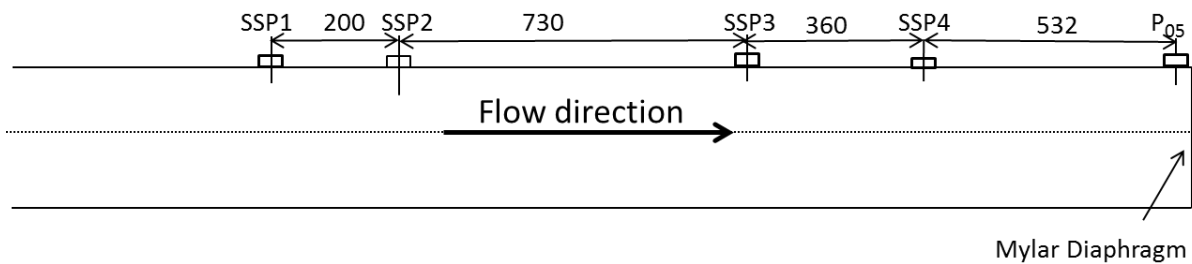


Fig. 2 Sensors location in shock tube. (All dimensions are in mm)

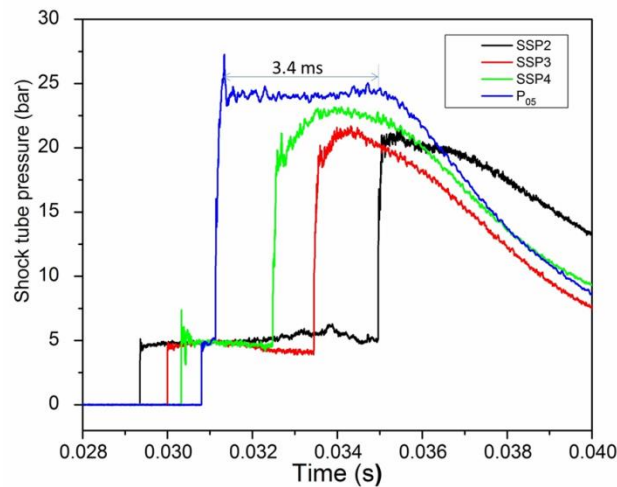


Fig. 3 Variation of static pressure with respect to time on shock tube

## 2. 2. Test Model

In the present investigation, sharp cone model is used as vehicle configuration. The model has provision to insert heat flux gauges and pressure measurement port as shown in Fig 4. The cone model has an apex angle of  $11.38^\circ$ , and its length is 2.450 D and base diameter is "D" mm. Due to manufacturing constraints a 'perfect' sharp cone isn't possible so the tip radius of model is 1.2 mm.. One half of the model is with platinum thin film gauges is named as G1 to G6 and the other half is with pressure port as S1 to S6. The base portion of model is with heat flux gauges and pressure port. It is marked as G7 to G9 and S7 to S9 respectively. The complete model is rotated ( $\phi = 180^\circ$ ), to find the windward and leeward heat transfer rate and surface pressure distribution.

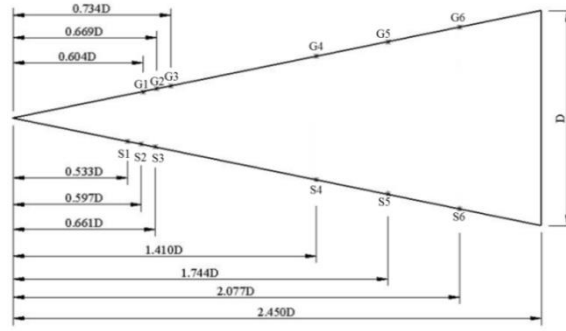


Fig 4. Sharp cone model used for experiments

Vacuum sputtering techniques used to deposit the platinum thin film sensors on the Macor substrate for heat flux measurements Saiprakash (2018). The rise in temperature due to the flow is sensed by the sensor as the change in its resistance. The sensor is supplied with a constant current, so that the change in voltage due to the change in resistance during the flow can be recorded by a data acquisition system. The sensors are connected through the analogue network circuitry, to the PC based data acquisition system. The details of the instrumentation used in heat transfer measurements along with the detailed data reduction methodology have been explained by Kevin M. Kinnear (1998). Thin film gauges are Calibrated based on the literature by Saiprakash et al (2018).

## 2. 3. Test condition

Experiments were carried out on the cone model at  $\alpha = 0^\circ$  and  $5^\circ$  at  $M = 6.56$  with angle of rotation of  $0^\circ$ ,  $90^\circ$  and  $180^\circ$  for both angles of attack. In the first test, the heat flux gauges were on the bottom surface of the model, pressure ports on the top portion of test model and then the test model was oriented  $180^\circ$  by the same incidence with the same condition to get the data in the other half of the model in the second test. The test condition and its uncertainty (D.J.Mee) are shown in Table 1.

Table. 1. Test condition during the present experiment.

$P_5$ (bar)	24.12( $\pm 5.1\%$ )
$M_s$	3.12( $\pm 1.2\%$ )
$h_0$ (MJ/kg)	1.2( $\pm 2.01\%$ )
$P_{inf}$ (Pa)	889( $\pm 6.9\%$ )
$T_{inf}$ (K)	152( $\pm 2.0\%$ )
$\rho_{inf}$ (kg/m <sup>3</sup> )	0.0203( $\pm 7.1\%$ )
$M_{inf}$	6.5( $\pm 0.7\%$ )

## 2.4. Test condition

Steady state flow field around the blunt cone model was simulated using Ansys Fluent code. SST k-omega turbulence model was used for CFD simulation. The structured mesh with finer grids near the walls was used to capture the shock pattern. The various boundary conditions used in the study are as follows: **Inlet:** The flow properties such as static pressure, static temperature and flow Mach number, were used for the CFD simulation. **Outlet:** At the outlet of computational domain, all

variables were extrapolated from interior domain. **Wall:** Blunt cone model surfaces were used as wall boundary condition. Both no-slip condition and constant temperature of 300 K were stated as wall boundary conditions. The target residuals to terminate the simulation were set at  $1 \times 10^{-5}$ . Grid independent study by varying the elements from 1.92 millions to 3.76 millions was carried out for the numerical study ; the changes in the calculated parameters for different grids were within  $\pm 3.4\%$ .

### 3. RESULT AND DISCUSSION

#### 3.1. Local heat transfer rate

The Experiment was carried out at flow Mach number of 6.5 at two different angles of attack. The heating rate and distribution of heating rate depends function of body shape and flight conditions. The heat flux was measured at bottom surface of model and surface pressure was measured at top surface of model . Then the model was rotated by  $180^\circ$  at same incidence with same test condition to get the data for the other half of the model.

At  $\alpha = 0^\circ$ , the variation of the heat flux along the surface for the sharp cone model is shown in Figs.8 where the experimental results are compared with the computational ones. The negative value of s/R is leeward side and positive value of s/R is windward side. The maximum surface heating rate occurs at stagnation point. This is due to large amount of kinetic energy dissipation occurrence at the stagnation point in the thin shock layer region at hypersonic free stream velocity. Because of very high temperature, the gas molecules dissociate in the shock layer and recombination which creates greater temperature gradient in the boundary layer, prominent to high heat transfer rates to stagnation point. The velocity gradient increases along the model surface from stagnation point due to three dimensional relieving effect.

The deviation in heat flux value occur mostly because of irregularity of groove-depth (e.g instead of 2.8 mm ,it is 2.9 or 2.7 mm) in the Aluminum diaphragm and also may be the cases where accumulation of moisture in the driver section. In addition to that minor Mylar diaphragm fragment could affect the flow quality. Due to this phenomena, the same quality and quantity of flow could not able to produced even though the tunnel was operated at same test condition.

At an axial location of 90.2 mm from the nose, the comparison of measured heat flux for  $0^\circ$  &  $5^\circ$  angle of attack shows that there is 26% increase in heat flux from windward and 52% reduction in heat flux from leeward. This clearly shows that the windward heating rate increases with angle of attack and leeward heating rate decreases with angle of attack. As angle of attack increases, maximum heating rate shift towards the windward side of the model. At  $\alpha = 5^\circ$ , windward heating is higher than when the model is at zero angle of attack. The shock layer thickness computed from Schlieren images using Matlab program .At  $s/D = 1$  from the nose, the decrease in shock layer thickness from  $\alpha = 0^\circ$  to  $\alpha = 5^\circ$  (windward) is 3.9% .Similarly for  $s/D = 2.5$  from the nose, the decrease in shock layer thickness is 4.42%.With increase the proximity of shock wave to cone surface, the windward heating rate is higher than model was mounted at  $\alpha = 0^\circ$ .

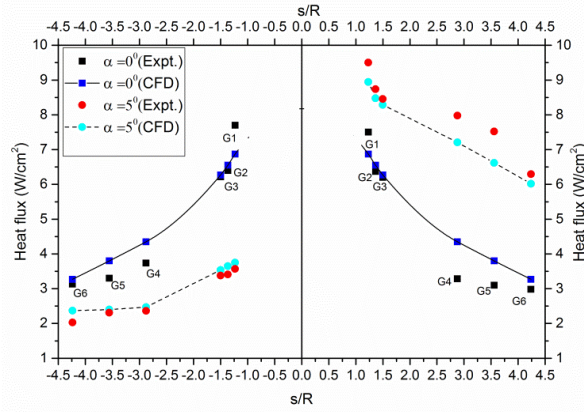


Fig 8. Distribution of convective heat transfer rate over the surface of sharp cone model for flow Mach number of 6.5

### 3.2. Pressure distribution

Heating rate is function of pressure gradient, local density, fluid temperature and state of the boundary layer. Pressure was measured along the surface of model at an angle of attack of  $\alpha = 0^\circ$ ,  $5^\circ$  like heat transfer was measured in a sharp cone model. At  $\alpha = 0^\circ$ , the experimental results slightly higher than computational as flow moves downstream of model as shown in Fig 9. The overall variation between the experimental and computation values is within 15%. The discrepancy of measured windward and leeward pressure distribution is about 10% for the same angle of attack. The surface pressure decreases along the flow direction like heating rate distribution for both angles of attack. At an axial location of 90.6mm from the nose, the comparison of measured pressure for  $0^\circ$  &  $5^\circ$  angle of attack shows that there is in 71% increase in pressure from windward and 45% reduction in pressure from leeward. The windward ray causes larger variation in pressure distribution with  $s/D$  (Fig 16) but leeward ray exhibit smaller variation in pressure distribution (Fig 17). For  $\alpha = 5^\circ$ , the measured circumferential pressure distribution decreases from windward ( $\phi = 0^\circ$ ) to leeward ( $\phi = 180^\circ$ ). At  $5^\circ$  angle of attack, both experimental and computational results are diverge by 8% and 6% for windward and leeward pressure distribution respectively. From the surface pressure and heating rate measurement, it is observed that both measurements reduces from the nose. Pressure change at  $\alpha = 0^\circ$  is 1.81, and for  $\alpha = 5^\circ$ , it is 3 and 0.7.

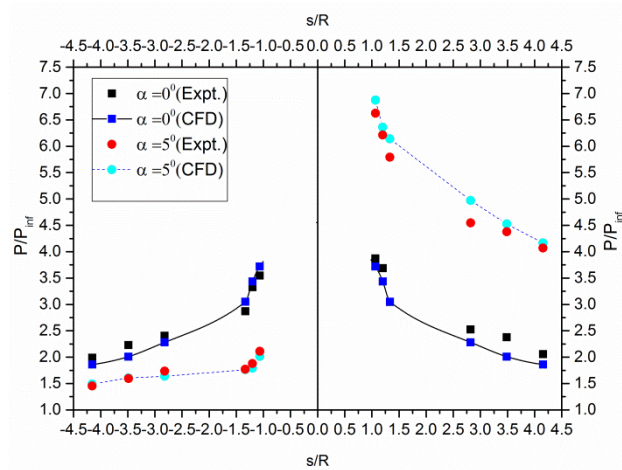


Fig 8 Variation of Pressure distribution over the surface of a sharp cone model for  $M=6.5$

### 4. Conclusion

The following results are concluded from the experimental, throretical and numerical data.  
-It is found that heating rate decreases along the model surface from the stagnation point.

-At  $s/D = 1$  from the nose, the decrease in shock layer thickness from  $\alpha = 0^\circ$  to  $\alpha = 5^\circ$  (windward) is 3.9%. Similarly for  $s/D = 2.5$  mm from the nose, the decrease in shock layer thickness is 4.42%. With increase the proximity of shock wave to cone surface, the windward heating rate is higher than model was mounted at  $\alpha = 0^\circ$ .

-At  $\alpha = 5^\circ$ , the windward heating rate is 2.5 to 3.5 times larger than leeward for the same test condition. The pressure distribution follows the same pattern as like heating rate.

-The changes in heat flux is higher for  $\alpha = 0^\circ$  is 4.5 and for  $\alpha = 5^\circ$  is 3.2 for windward ray. The changes in Pressure distribution along stream wise length for  $\alpha = 0^\circ$  is 1.81, and for  $\alpha = 5^\circ$ , it is 3 and 0.7 for windward and leeward ray respectively.

-At  $\alpha = 0^\circ$ , the maximum base heat flux is 7% of windward heating at  $s/D = 0.6$  and Peak base pressure is 10% of windward pressure distribution at same location.

## References

1. H.G. Hornung, 28<sup>th</sup> Lanchester Memorial Lecture-Experimental real-gas hypersonics, Aeronautical Journal, 379-389 (1988).
2. M. Tauber, Mars Environmental Survey Probe Aero brake Preliminary Design Study, Journal of Spacecraft and Rockets, 30(4), 431-437(1993).
3. J.R. Micol, Aerothermodynamics measurement and prediction for a modified orbiter at Mach 6 and 10 in air, Journal of Spacecraft and Rockets, 32, 737-748(1995).
4. M. Tauber, Mars Environmental Survey Probe Aero brake Preliminary Design Study, Journal of Spacecraft and Rockets, 30(4), 431-437(1993).
5. I.S. Raju, and W.J. Craft, Analysis and Sizing of Mars aero brake Structure, Journal of Spacecraft and Rocket, 30(1), 102-110(1993).
6. L. De Luca, G. Guglieri, G. Cardone and G.M. Carlomagno, Experimental analysis of surface flow on a delta wing by infrared thermography, AIAA Journal, 33, 1510-1512(1995).
7. J.P. Hubner, B.F. Carroll, K.S. Schanze, H.F. Ji and M.S. Holden, "Temperature- and Pressure-Sensitive Paint Measurements in Short-Duration Hypersonic Flow, AIAA Journal, 39, 654-659(2001).
8. Chandra, T.K., Shanmugam, V., Janardhana Rao, P., Ravi J. Prasad, Treena Sen Gupta, Prakash, S., and Narayana, A.S., 2007, Commissioning of 1m diameter shock tunnel at DRDL, In: Challenges in High Speed Transatmospheric Air & Space Transportation, Hyderabad.
9. Kevin M. Kinnear, and Frank K. Lu, Design, calibration and testing of transient thin film heat transfer gauge, 20th AIAA Advanced Measurement and Ground Testing Technology Conference, Fluid Dynamics and Co-located Conferences (1998). doi: 10.2514/6.1998-2504.
10. M. Saiprakash, C. Senthil Kumar, G. Balu, V. Shanmugam, Singh Prakash Rampratap, G. Kadam sunil. Convective heat-transfer rate and surface pressure distribution over a cone model at hypersonic speeds, Proc. IMech Part G Journal of Aerospace Engineering (2018)
11. D.J. Mee Uncertainties Analysis of Conditions in Test Section of the T4 Shock Tunnel, University of Queensland, Centre for Hypersonic Research Report No. 4/93, Australia (1993).